small NANO MICRO

Nanoclusters

DOI: 10.1002/smll.200700276

Zinc Porphyrin-Driven Assembly of Gold Nanofingers

Valentina Arima, Robert I. R. Blyth, Francesca Matino, Letizia Chiodo, Fabio Della Sala, Julie Thompson, Tom Regier, Roberta Del Sole, Giuseppe Mele, Giuseppe Vasapollo, Roberto Cingolani, and Ross Rinaldi*

***N**anofingers of gold covered by porphyrins are prepared by a combination of atomic manipulation and surface self-organization. A submonolayer of zinc(II) 5,10,15,20-tetrakis(4-tert-butylphenyl)-porphyrin (ZnTBPP) axially ligated to a self-assembled monolayer of 4-aminothiophenol (4-ATP) on Au(111) is prepared and studied using a combination of ultrahigh vacuum techniques. Under the electric field produced by the STM tip, the relatively weakly bound Au surface atoms along the discommensuration lines become mobile due to the strong bond to 4-ATP, while the tendency of the porphyrins towards self-assembly result in a collective motion of gold clusters. The clusters diffuse onto the surface following well-defined pathways along the* $[11\bar{2}]$ *direction and then reach the step edges where they assembled, thus forming nanofingers. First-principles density functional theory calculations demonstrate the reduction of the binding energies between the surface gold clusters and the substrate induced by adsorption of thiols. Scanning tunneling microscopy images show assemblies across three adjacent discommensuration lines of the Au(111)-(22 ×* $\sqrt{3}$*) reconstruction, which collectively diffuse along these lines to form islands nucleated at step edges.*

Keywords:
- nanofingers
- porphyrins
- scanning tunneling microscopy

1. Introduction

Porphyrins and gold nanowires are both of great interest in optoelectronics for different reasons. The unique optical, photoelectrochemical, and chemical properties of such molecules together with their tendency to form ordered structures in the solid state,[1] have already been exploited in a number of devices.[2–10] Gold nanowires are now emerging as interconnections or active components[11] in nanodevices because of their capability to increase the spectroscopic response from chromophores adsorbed on them[12]. The combination of porphyrins with gold nanowires seems to be an attractive formula for efficient optoelectronic devices. An important issue is how to fabricate gold nanowires covered by porphyrins.

Although gold microwires covered by laser dye are easily fabricated and appear to form efficient devices,[12] the preparation of gold nanowires covered by chromophores is rather difficult because of their low stability at room temperature.[11] One-dimensional (1D) nanowires have, however, already been produced by depositing 0.15 ML of

[*] Dr. V. Arima, Dr. R. I. R. Blyth, Dr. F. Matino, Dr. L. Chiodo, Dr. F. D. Sala, Dr. J. Thompson, Prof. R. Cingolani, Prof. R. Rinaldi
National Nanotechnology Laboratory (CNR-INFM)
Distretto Tecnologico ISUFI
Università degli studi di Lecce
via Arnesano, 73100 Lecce (Italy)
Fax: (+39) 083-229-8180
E-mail: valentina.arima@unile.it

Dr. R. I. R. Blyth, Dr. T. Regier
Canadian Light Source
101 Perimeter Road
University of Saskatchewan
Saskatoon, S7N 0X4 (Canada)

Dr. J. Thompson
Department of Chemistry
University of Western Ontario,
London, Ontario, N6A 5B7 (Canada)

Dr. R. Del Sole, Dr. G. Mele, Prof. G. Vasapollo
Dipartimento di Ingegneria dell'Innovazione
Universita' degli Studi di Lecce
via Arnesano, 73100 Lecce (Italy)

gold on Si(111), as confirmed by scanning tunneling microscopy (STM) and photoemission spectroscopy.[11a]

Recently, Yin et al.[13a] reported the possibility of producing ''gold fingers'' on the (111) gold surface by structuring the Au(111) surface at the nanometer scale with an STM tip. It seems that local atomic diffusion can be induced on the Au surface since the activation energy is reduced by applying a voltage pulse to the tip. The second-layer atoms are exposed by physically extracting top-layer atoms with an STM tip. After the removal of the top-layer gold atoms from a step edge, the step does not recede uniformly and stripes of a few nanometers width are formed.

The mobility of gold atoms is also increased when aromatic thiols[14] are immobilized on the surface because the strong Au–S bond weakens the adhesion between the surface Au atoms and the underlying layers. The mobile Au atoms aggregate and form islands. The strong intermolecular interactions favor aggregations of the adsorbed aromatic molecules, each with an Au atom attached, into islands.

In this work, we immobilized a submonolayer of the chromophore zinc(II) 5,10,15,20-tetrakis(4-*tert*-butylphenyl)-porphyrin (ZnTBPP) by means of an aromatic thiol monolayer, 4-aminothiophenol (4-ATP) self-assembled monolayer (SAM), on the Au(111) surface, and then gold clusters bound to the molecules were moved under the electric field produced by the STM tip. The molecular formulas and the scheme of the 4-ATP/ZnTBPP complex assembled on the gold surface are shown in Figure 1. Since the bond of thiols to gold seems to weaken the interaction between the surface Au atoms and the underlying layers[14] and 4-ATP/ZnTBPP is a very stable pyramidal square complex,[15] which can be easily polarized by the tip field,[16a] we suggest that the gold clusters linked to the molecules could be moved by a tip field weaker than that required for nonfunctionalized gold.

In order to verify that the thiol–cluster bond reduced in some way the interaction between the cluster itself and the substrate, inducing therefore a higher mobility of the cluster, we performed first-principles density functional theory (DFT) calculations.

In some theoretical studies[17–19b] diffusion of small clusters on different (111) and (001) surfaces has been investigated and described by embedded atom models and molecular dynamics, thus determining energy barriers along different diffusion paths and studying dynamic features such as collective motion of groups of atoms in the cluster,[17–19b] rolling for spherical clusters[18] and internal motions inside the clusters themselves.[19] However, these models could not be easily applied to our case because they don't take into consideration that molecules absorbed on clusters strongly affect their mobility. As a consequence, a ''static'' approach, reporting some structural, energetic and electronic properties of bare clusters or thiol-covered clusters adsorbed on gold, has been used in this work to simulate in a simple way the complex experimental structure. Our model relies on the observations that i) adsorbed clusters are mainly monolayers and ii) the thiol-bond effect is localized around the region of the S–Au bond. We used a monoatomic small gold cluster adsorbed on an Au(111) surface, and a small thiol molecule, methanethiol, to mimic the whole (4-ATP) SAM/cluster/Au(111); we found

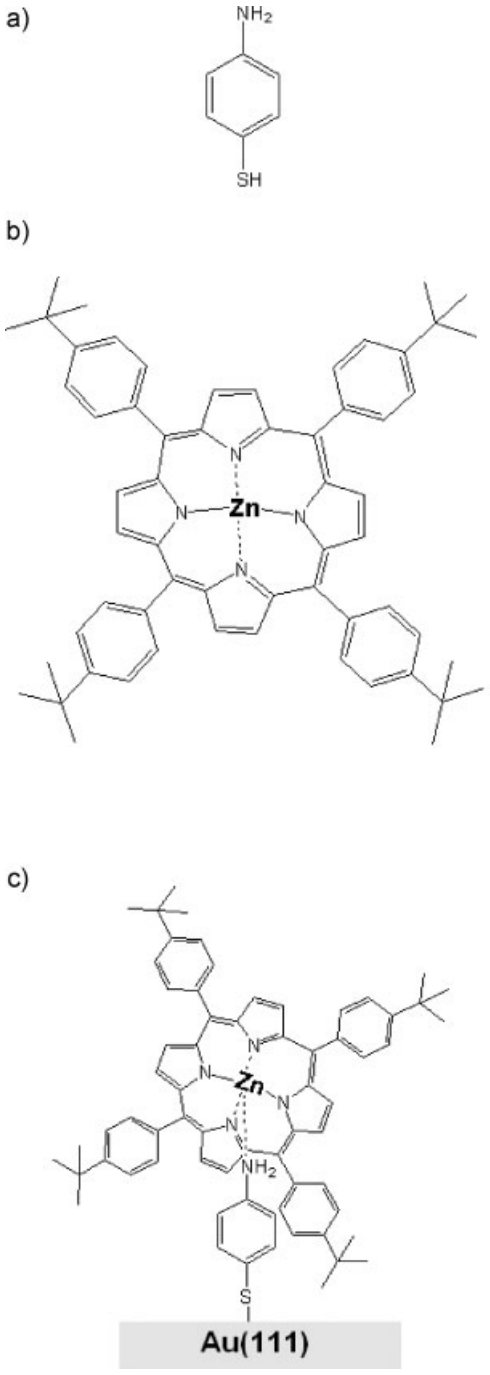

Figure 1. Molecular structures of a) 4-aminothiophenol (4-ATP) and b) zinc (II) 5,10,15,20-tetrakis(4-tert-butylphenyl)-porphyrin (ZnTBPP). c) Scheme of the 4-ATP/ZnTBPP complex on the gold surface.

that the increased mobility of the gold clusters functionalized by the molecules is in fact consistent with a reduction of the interaction between the cluster itself and the substrate.

The selective transport of gold clusters linked to 4-ATP/ZnTBPP and the assembly process of functionalized gold nanowires were experimentally followed and characterized by scanning tunneling microscopy (STM) and spectroscopy (STS),[20] synchrotron-radiation-excited photoemission spectroscopy (PES), and near-edge X-ray absorption fine structure

small NANO MICRO

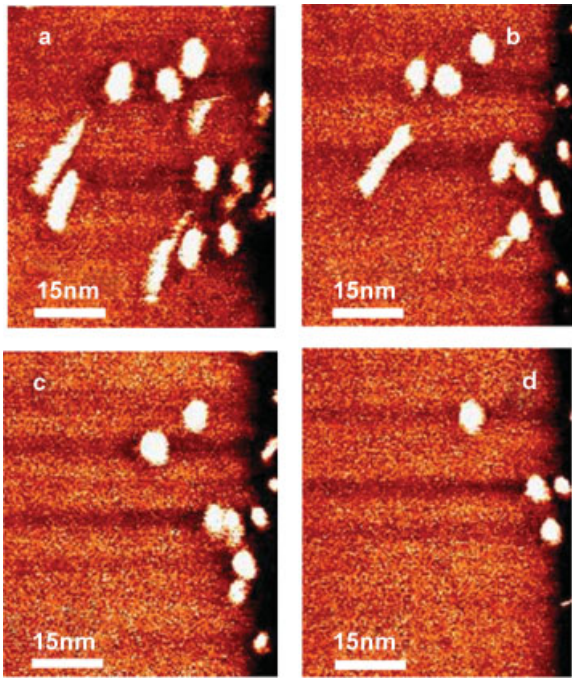

Figure 2. Time evolution of the islands at a) 0, b) 6, c) 12, and d) 18 min. STM images acquired at 0.2 V, 0.8 nA.

(NEXAFS).[21] Finally, gold nanowires covered by ZnTBPPs were successfully isolated at the step edges.

The bare gold (111) substrate has been characterized without molecules and with a 4-ATP SAM in our previous paper.[16b,c] The interaction of the thiol SAM with Cobalt (II) 5,10,15,20-tetrakis(4-*tert*-butylphenyl)-porphyrin (CoTBPP) has also been investigated.[16a,c] In the case of ZnTBPP, the STM images showed assemblies across three adjacent discommensuration lines of the Au(111)-$(22 \times \sqrt{3})$ reconstruction, which collectively diffused along these lines, to form islands nucleated at step edges. The tunneling conditions used, the acquired STS spectra, and the apparent heights observed suggest that gold clusters, rather than organic molecules, are being directly imaged. The noisy structures near the step edges at higher voltages and the corresponding STS spectra suggest that the clusters, mobile on the surface, are covered by molecules. PES and NEXAFS measurements showed that ZnTBPPs are chemisorbed on the surface without a preferred orientation of the porphyrin ring and induce a significant distortion of the gold local electronic structure. We suggest that the relatively weakly bound Au surface atoms linked to the 4-ATP/ZnTBPP complex become strongly mobile at very low (tip) electric fields, while the tendency of the molecules towards self-assembly[4] results in the observed collective motion.

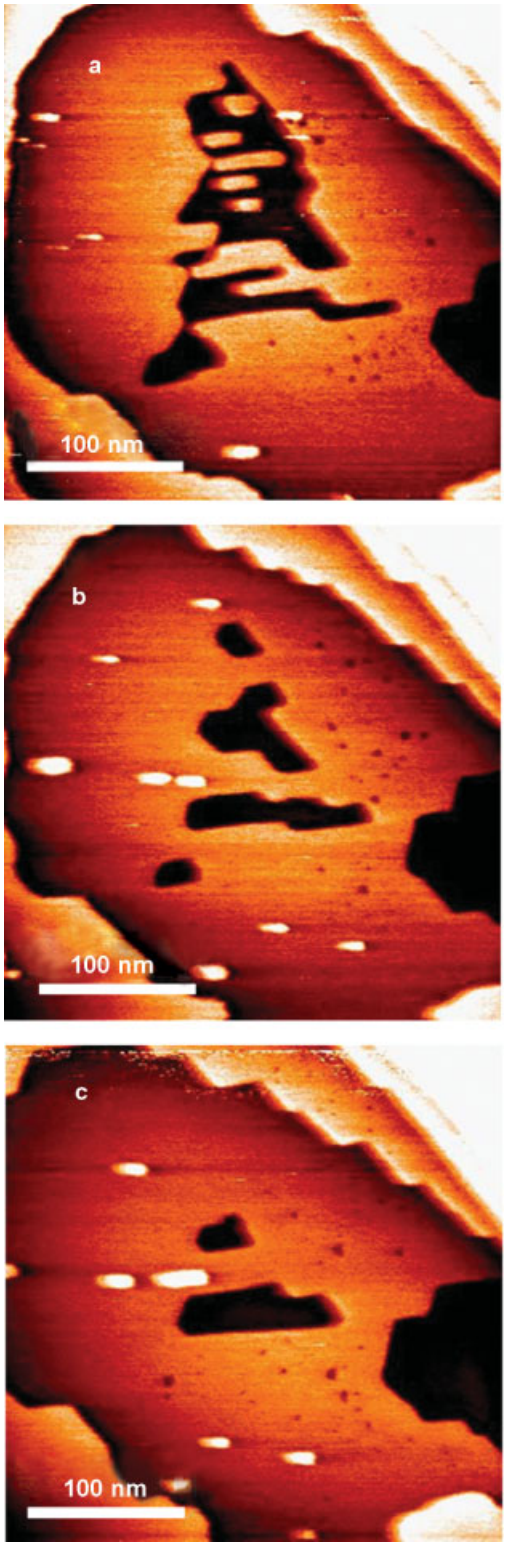

Figure 3. Evolution processes near the step edges at a) 0, b) 5, and c) 10 min. STM images acquired at 0.2 V, 0.5 nA.

2. Results

2.1. Experimental Results

In the STM images here reported and acquired on an Au(111) sample functionalized by 4-ATP and ZnTBPP molecules, small clusters moving along the surface and modifications occurring at the step edges can be observed. The movement is induced by the tip field as already shown by Guo et al.[13b] We believe that Au islands covered by molecules move onto the

surface and then reach the step edges as suggested by STM and STS measurements, thus creating new structures near the steps. This is supported by several observations, which we report in the following.

The apparent height of the islands shown in Figure 2 is about 2.3 ± 0.4 Å, which corresponds to the height of a single Au atomic layer. The clusters have lateral dimensions of 4.86 ± 0.53 nm and 7.89 ± 0.80 nm. Some of them appear elongated thus forming stripes of variable dimensions. The shape of the clusters doesn't appear related to the features of the substrate.

We studied the formation of the islands with real-time STM by acquiring consecutive images on the same area. Each scan took about 6 min. If we observe the structures in Figure 2 it seems that the sizes of the clusters don't change too much but the number of the islands and stripes decreases gradually in this area. In another area of the sample more regular clusters were found and they appear essentially 4.07 ± 0.62 nm wide, 10.84 ± 1.89 nm long, and 2.2 ± 0.2 Å high. The tip effect and diffusion phenomena can influence the shape and the lateral dimensions of the clusters, thus giving apparent different features to the islands.

From the images in Figure 2 it is not easy to understand why the islands disappeared and where they moved to. A possible explanation comes from other images acquired in sequence near the step edges (see Figure 3). Each scan took about 5 min. Au-surface step edges expand when the nearby islands dissolve because the Au atoms in the islands are being incorporated into the steps. Some islands of size similar to those previously described move along the surface and, finally, reach the step edges where they are dissolved, thus inducing an expansion of the step edges. The surface is continuously modified and holes of different size but with a depth of about 1.6 ± 0.3 Å can continuously open and close in several positions of the sample.

All the above images were acquired at 0.2 V, a voltage for which only gold and not molecules can be reasonably visualized. In looking for the molecules, the voltage was varied until noise in some regions appeared. In the two insets of Figure 4, two images acquired in sequence at different voltages are shown. The area shown in the inset of Figure 4a was imaged at 0.2 V and 0.8 nA, while that in Figure 4b was acquired at same set point current but at a voltage of 1 V. On increasing the voltage, in the region of the image indicated by the blue rectangular box a noisy pattern appeared, while in the other parts the scanning was undoubtedly more stable and quite similar to the image recorded at low voltages.

The STS characteristics extrapolated from a grid of points collected in the same area reflect this phenomenon (see Figure 4). In the two curves of Figure 4a, averages of spectroscopic points acquired respectively in the regions indicated by the rectangular boxes (see image in the inset), a behaviour typical of metals and due to the conduction of gold can be recognized. The two curves of Figure 4b were extrapolated respectively from the noisy region indicated by the blue rectangular box (blue line) and from the region indicated by the black rectangular box (black line) of the image shown in the inset and acquired at 1 V and 0.8 nA. No zero-current region, characteristic of semiconductor behavior,

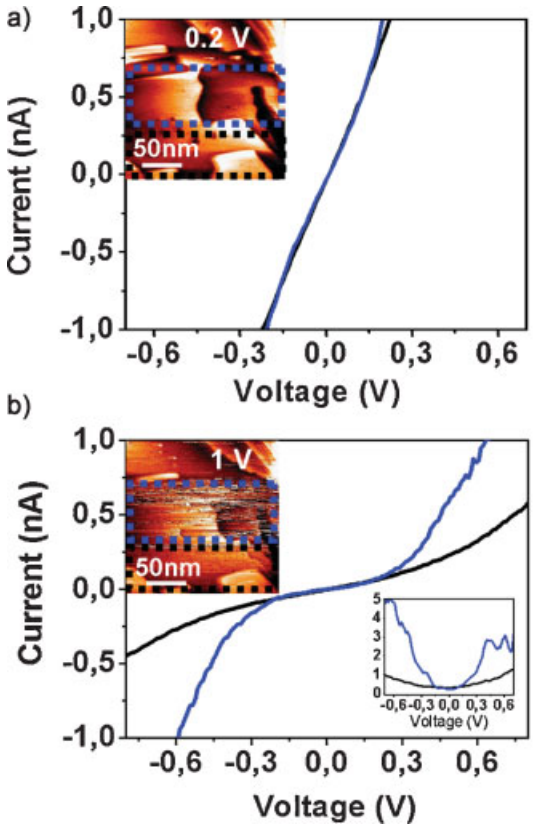

Figure 4. STS curves acquired at a) 0.2 V, 0.8 nA and b) 1 V, 0.8 nA. The blue and black curves were acquired in the areas indicated by the rectangular boxes. STM images shown in the insets were acquired at a) 0.2 V, 0.8 nA and b) 1 V, 0.8 nA. In the second inset of (b) are the normalized conductance curves corresponding to the curves shown in (b).

can be recognized in the black curve. The curve is featureless and essentially due to the conduction of gold. The STS features of the noisy region of the image (blue line) are quite different since the negative and positive currents start increasing at ± 0.3 V, approximately where the corresponding normalized conductance curve (the blue line in the inset) shows some peaks. We suggest that the blue curve is a combination of the gold and ZnTBPP features and therefore the zero-current region cannot be directly related to the HOMO–LUMO gap of ZnTBPP[29] (HOMO: highest occupied molecular orbital; LUMO; lowest unoccupied molecular orbital). It is possible also to hypothesize that in the region of the image (inset of Figure 4b) indicated by the blue rectangular box, where STM images show phenomena suggesting high cluster mobility, the noise indicates molecules acting on the surface. In the other part of the image, where the mobility is reduced, few molecules are present and the acquired STS characteristic is essentially due to the gold surface.

On a more crystalline Au(111) sample we clearly observed the formation of gold stripes a few nanometers in width. Figure 5a shows that, after the deposition of ZnTBPP on the 4-ATP-functionalized Au(111) surface, well-defined assemblies of regular shape and dimensions appear on a regular $22 \times \sqrt{3}$ surface reconstruction. The assemblies were observed

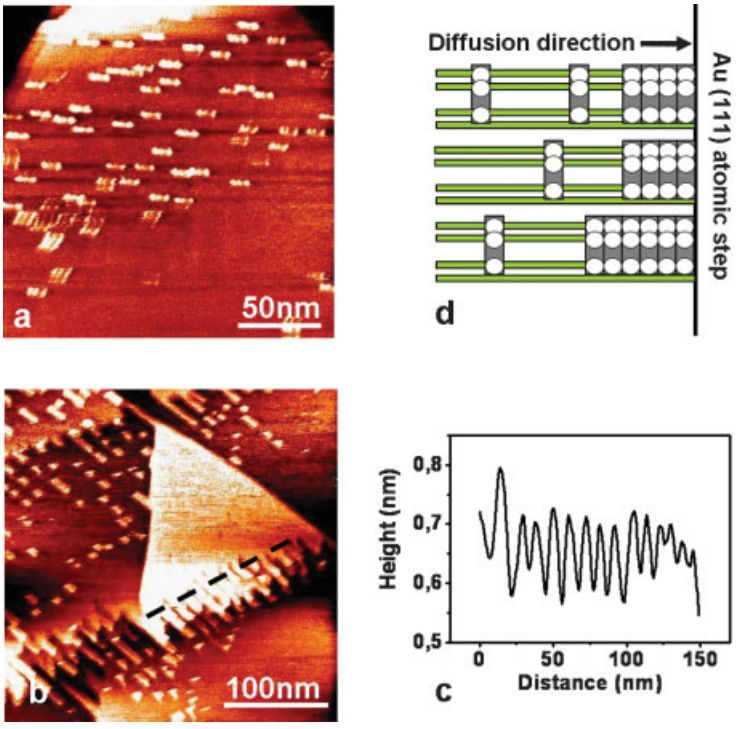

Figure 5. Typical unfiltered STM images of Au(111) functionalized by 4-ATP and ZnTBPP a) on a terrace acquired at 0.2 V, 0.5 nA; b) at the step edge acquired at 0.2 V, 0.5 nA. c) Line scan along the line shown in (b); d) schematic diagram of the observed molecular diffusion.

to move on the thiol-functionalized surface, following well-defined pathways along the $[11\bar{2}]$ direction. We suggest that the ''streaking'' of the images in the lower part of Figure 5a is due to the motion of these assemblies during the timescale of the scan, rather than accumulation of multiple assemblies. The assemblies are 3.87 ± 0.71 nm wide, 12.71 ± 0.60 nm long, and 1.9 ± 0.3 Å high. Though they appear different, these clusters can be associated with those previously described. More detailed information about the features of these clusters and their movements can be extrapolated from these images. The observed structures seem to consist of three basic units, with a separation between the first and third units of 8.09 ± 0.42 nm and between the first and second units of 2.87 ± 0.47 nm. Considering that unlike true single-crystal gold, the thin Au(111) films used here can show reconstruction line spacing ranging from 6.3 to about 9.0 nm;[30] the distances between the units of the clusters appear closely related to the periodicity of the underlying surface reconstruction and to the distance between two nearest-neighbor parallel discommensuration lines. Moreover, the molecular spots appear (Figure 5a) more defined near the step edge of the gold terraces and more elongated along the diffusion direction far from the step edge, thus suggesting that the ''speed'' of their motion is related to their position with respect to the edge.

In the vicinity of a step-edge the density of molecular units, Figure 5b, is much higher and there is clearly 2D island formation, and a well-defined diffusion direction. A line scan along across neighboring 2D islands is also shown in Figure 5c. In order to cross a large number of 2D islands this line scan is at an angle of ≈30° with respect to the $[\bar{1}10]$ direction, and the distance scale has been corrected to take this into account. From this the periodicity of the adjacent minima can be determined to be ≈9.17 nm, which, given the uncertainties in this measurement, is again consistent with the periodicity of the underlying Au(111)-$(22 \times \sqrt{3})$ reconstruction.

Since it was possible to clearly image the fingers on a less crystalline sample and simultaneously resolve the herringbone reconstruction, the possible directions of the fingers were identified.

The long axis of some fingers shown in Figure 6 makes a 145° angle to the discommensuration lines on the terrace. It has been verified, by changing the fast-scan direction by 45°, that this parameter doesn't affect the direction of the fingers. It seems that the fingers prefer to align in this way, as already shown by Guo et al.[13b] Fingers perpendicular to the discommensuration lines have also been observed, as illustrated in Figure 6. The directions of bare gold fingers on Au(111)[13b] were found to be in good agreement with those described here, thus confirming that the observed phenomena have a common origin.

Clear evidence of the presence of ZnTBPP, and its influence on the gold electronic structure, is shown in the photoemission and N K NEXAFS spectra in Figures 7 and 8.

Figure 7a shows the Au NNV Auger peak and the Zn 2p photoemission peaks. The 2p is the highest-intensity photoemission peak for Zn but sits on an intense secondary electron background due to the Au N shell photoelectrons; observing

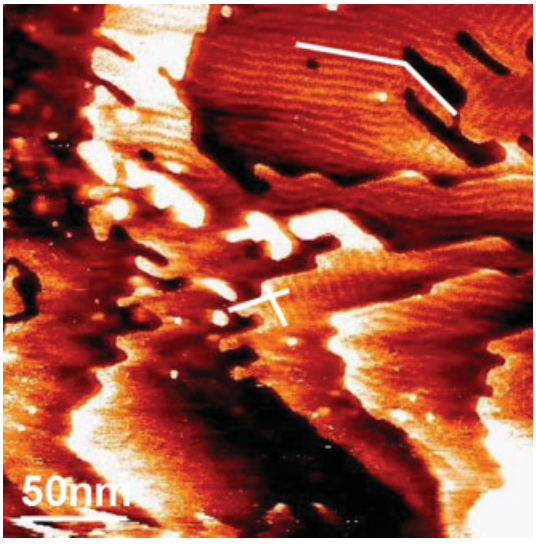

Figure 6. Typical unfiltered STM image of the Au(111) reconstruction.

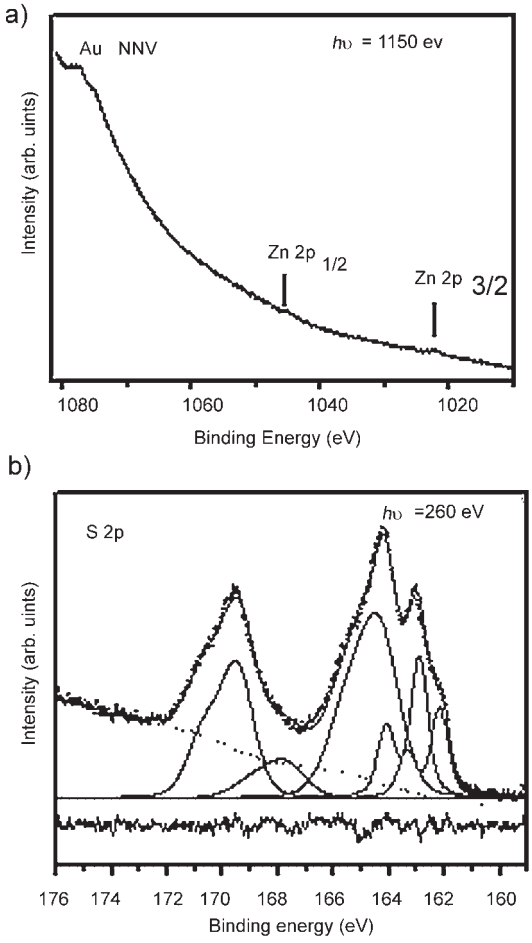

Figure 7. a) Spectrum of the Au NNV Auger and Zn 2p photoemission peaks of Au/4-ATP/ZnTBPP, excited using high-intensity undulator synchrotron radiation; b) high-resolution S 2p photoemission spectrum of Au/4-ATP/ZnTBPP.

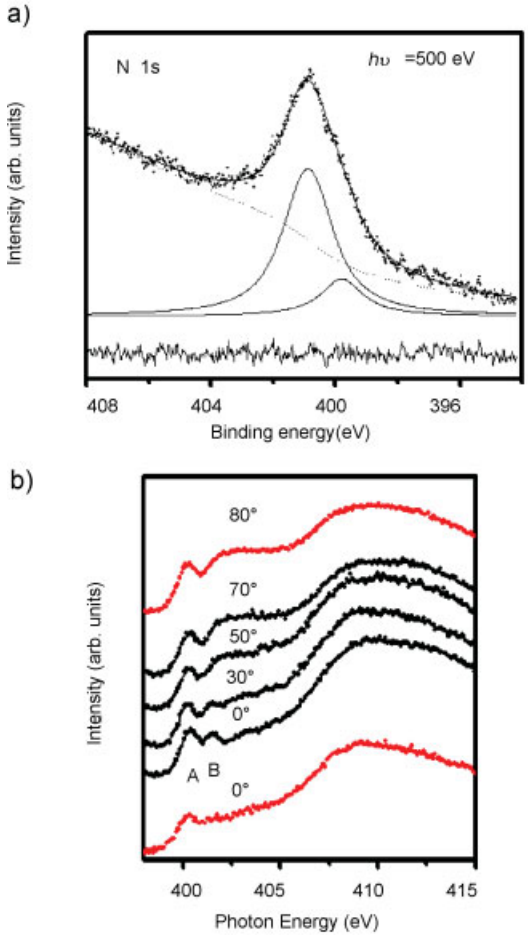

Figure 8. a) High-resolution N 1s photoemission spectrum of Au/4-ATP/ZnTBPP; b) nitrogen K edge NEXAFS spectra of Au/4-ATP/ZnTBPP (black curves) as a function of the incidence angle (relative to the surface normal). Also shown are spectra of Au/4-ATP (red curves) at grazing and normal incidence, from Reference [16b].

the Zn peaks is thus nontrivial. We were unable to resolve these peaks on the (bending magnet) BEAR beamline. The spectrum of Figure 7a was taken using a wide exit-slit setting on the SGM undulator beamline, with a correspondingly high photon flux of $\approx 10^{12}$ photons s^{-1}. This is almost certainly sufficient to damage the film but does serve to conclusively demonstrate the presence of the porphyrin on the surface. It is clear from the quality of the data of Figure 7a why attempts at higher resolution spectroscopy, with correspondingly lower flux, did not result in useful data.

The sulfur 2p photoemission spectrum is shown in Figure 7b, together with the results of a curve fit, using similar parameters to that of Au/4-ATP.[16b] The spectrum is analogous to that observed for Au/4-ATP, showing a number of different components as discussed elsewhere,[16b] but here it is better resolved, allowing a more reliable determination of peak widths. The width of the component bonded directly to Au, at a $2p_{3/2}$ binding energy of 162.1 eV[16b] is found to be only 0.6 eV and appears well defined. This is in contrast to the value of 1.8 eV found for Au/4-ATP, and suggests the presence of a single S–Au species, rather than the multiple sites speculated in Reference [16b]. Although the resolution in the present experiment is rather higher, this improvement alone cannot account for the observed difference in width.

The N 1s photoemission spectrum is shown in Figure 8a, together with the results of a curve fit. Here the presence of two components is indicated, as is also evident from a visual inspection of the raw data. The lower energy of the two components, at 399.6 eV, corresponds to the value for 4-ATP,[16b] while the higher-energy component corresponds to the porphyrin.[16a] The presence of only one porphyrin-related N 1s peak is indicative of a metal porphyrin, since metal-free porphyrin displays a double N 1s peak due to protonated and unprotonated nitrogen species.[31] The presence of a significant 4-ATP contribution to the N 1s peak is in contrast with the observations for Au/4-ATP/CoTBPP, where a full monolayer was implied, and is consistent with the apparent submonolayer coverage seen in the STM data.

Nitrogen K-edge NEXAFS spectra of Au/4-ATP/ZnTBPP (black curves) are shown in Figure 8b. The NEXAFS spectra of metal-porphyrins display a double peak around 400 eV due to the unoccupied π^* resonances.[32] These are labeled as A and B in Figure 8b. In the event of a preferred orientation of the porphyrin ring, the intensities of these peaks should show

small

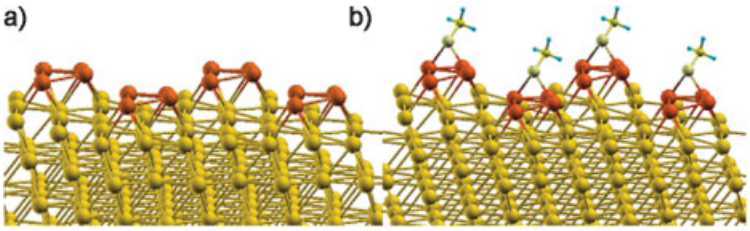

Figure 9. a) 4-Au atoms cluster adsorbed on Au(111) and b) the same system with methanethiolate molecules adsorbed in the bridge site for each cluster.

considerable variation with the incidence angle of the photon beam. Figure 8b shows that there is indeed angular variation in the NEXAFS spectra. However, the spectra are a superposition of both ZnTBPP and 4-ATP signals. The NEXAFS spectra of Au/4-ATP (red lines) also show significant angular variation,[16b] as indicated by the two spectra of Au/4-ATP included in Figure 8b. From a comparison of these spectra with those of Au/4-ATP/ZnTBPP it appears that the angular variation seen in the latter spectra may be due entirely to the 4-ATP molecules. Further, the intensity of peak A does not show any angular variation. It therefore implies that there is no preferred orientation of the ZnTBPP molecules.

2.2. Theoretical Results

Since the thiol–gold interaction has a local character, i.e. it is localized around the region of the S–Au bond, we chose both a small adsorbed molecule and a small gold cluster to describe large organic molecules on large-area clusters, always preserving the energetic bond description.

We computed the binding energies for the different analyzed systems using the formula

$$E_b = (E_{sub} + E_{ads}) - E_{tot}$$

where E_b is the binding (or adsorption) energy, E_{sub} is the energy of the relaxed substrate system, that is, the gold slab (in the following denoted by S) or the nanocluster (N) or the cluster/slab system (NS), and E_{ads} is the energy of the relaxed adsorbate, that is, the isolated thiolate molecule CH_3S (denoted by M) or the nanoclusters (N) or the whole thiolate/cluster adsorption unit (MN). Finally, E_{tot} is the energy of the relaxed full system.

The relaxed configurations for the gold nanoclusters on gold surface (NS) and for the thiol plus gold nanoclusters on gold surface (MNS) are shown in Figure 9a and b, respectively.

Table 1. Binding energies in eV for various subsystems (see text for details).

	This work	Others
M–S	1.87	1.73,[27] 2.3[33]
M–N	2.76	3.3[33]
M–NS	2.06	–
N–S	4.11	–
MN–S	3.41	–

The computed Au–S bond (MN–S) is 2.45 Å (and 2.48 Å for the thiol on gold surface; see also the value 2.50 Å in Reference [27]), and the S–C bond is 1.84 Å. The angle between the molecular axis and the normal to the surface, which is 58.62° in the thiol/surface case,[34] is tilted to 59.85° for the thiol/cluster/substrate system.

The calculated binding energies for different subsystems are reported in Table 1. We obtain an adsorption energy of thiolate on bare gold (M–S) of 1.87 eV, in good agreement with available experimental data, 1.7 ± 0.2 eV,[35] and comparable with previous theoretical data, 1.73 eV [27] and 2.3 eV.[33] This binding energy increases to 2.76 eV for the molecule adsorbed on the isolated cluster (M–N) (3.3 eV in Reference [33]), and to 2.06 eV for the molecule adsorbed on the cluster/surface system (M–NS). Therefore, the M–N bond, even if lowered in energy by the substrate presence, is stronger than the pure M–S interaction by 9.7%. The calculated adsorption energy for the N–S is 4.11 eV, and this energy decreases to 3.41 eV when a thiol is adsorbed on the cluster (MN–S), with a variation of 19% in bond strength.

Figure 10 shows the charge-density variations for NS and MNS along the direction z normal to the surface, averaged on the surface plane: the 3D charge-density difference for NS (above) and MNS (below) are also plotted. Figure 10 clearly shows that the presence of the adsorbed thiol modifies the charge distribution. In fact, part of the electron-density

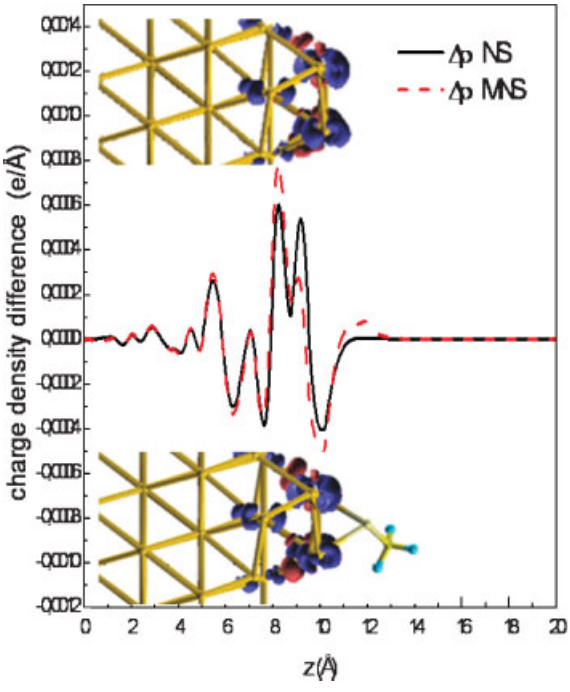

Figure 10. Central panel: charge-density difference along the direction normal to the surface, for the cluster/slab system (solid black line) and with a CH_3S molecule adsorbed (dashed red line). Top and bottom panels: the charge-density difference spatial distribution for cluster/slab (NS), and thiolate/cluster/slab (MNS), respectively, with red clouds denoting regions of electron accumulation (negative charge) and blue denoting electron depletion (positive charge).

accumulation, initially localized on the adsorbed cluster, is shifted toward the cluster/slab bond, while part is shifted on the molecule.

3. Discussion

Since the STM voltages used are too low to visualize the orbitals of either 4-ATP or ZnTBPP, and the apparent height of the observed structures is very similar to the step height of Au(111), it appears that the part of the structures that is being imaged consists of gold atoms or clusters that have been pulled out of the topmost surface layer. This may be supported by the S 2p photoemission spectra, which appear to show a considerably more well-defined S–Au bond than was the case for Au/4-ATP, where multiple absorption sites on the herringbone reconstruction are possible. All the STM images acquired clearly show clusters of gold atoms and surface modifications at the step edges. It seems that these phenomena are correlated. Despite small differences in the shape of the clusters, their origin and destination seem unequivocal: Au islands covered by molecules move onto the surface following precise pathways and then reach the step edges, thus creating new structures near the steps. These structures show at atomic level the typical herringbone reconstruction of Au(111). The photoemission and nitrogen K-edge NEXAFS spectra confirm that 4-ATP and ZnTBPP molecules are, in fact, present on the surface. At the same time, STS and voltage-dependent STM images suggest that molecules are located mainly at the step edge, where the phenomenon of cluster mobility appears more evident, and determines the growth of the fingers.

The apparent diffusion seen in Figures 2–5a could be caused by a combination of different effects. Theoretical calculations show that methanethiolate through the strong Au–S bond reduces the adhesion between the gold adatoms and the substrate. Due to the local character of the Au–S bond, these theoretical results can be assumed to be valid for all sulfur-anchoring organic molecules such as the aromatic thiols (4-ATP) used in the experiments. In addition, in our case, the surface Au atoms become much more mobile than the atoms on bare Au surfaces due to the interaction between adjacent molecules, which aggregate and form islands. A comparison of the 2D islands in the upper part of Figure 5a with the ''streaking'' in the lower area of the same figure further suggests that what is seen in the latter images is in fact diffusion. Molecular diffusion on the surface can be understood if we consider Figure 5a as the initial phase and Figure 5b as the final phase of the molecular migration. This is shown schematically in Figure 5d.

Collective movements of gold clusters covered by aromatic thiols (4HP)[14b] and their incorporation at the step edge have been already followed by STM in a liquid environment. This case saw the phenomenon of coalescence of islands of similar size into bigger ones and exclusion of the tip effect. In our images, and particularly in Figure 5a, the assemblies don't change their shape during the experiment but only diffuse along the surface.

If thiols are responsible for the high mobility of the gold atoms, the porphyrins, which can strongly interact with each other by π–π interactions,[36] could influence the assembly of the units. It is not clear why the self-assemblies consist of three, rather than four or more, units on neighboring discommensuration lines. It is possible that the actual size of the assemblies is slightly larger than the periodicity of the underlying reconstruction, as discussed earlier, in which case there would not be space for a fourth unit.

However, despite these difficulties in the explanation of how randomly oriented ZnTBPPs interact on the top of the clusters — which is also unclear in the case of gold clusters covered by 4HP — there is a significant difference between our assemblies and those described by Guo et al.;[14b] our assemblies don't modify their shape during the STM timescale and move very fast compared with the islands shown in Reference [14b]. Our islands disappeared in about 5 min (see Figure 2), while the 4HP islands slowly move or modify their shape, on a timescale of 30 min. It seems that our assemblies haven't the time to change their shape because the relatively fast movement towards the step, facilitated by the discommensuration lines, limits interaction between them before reaching the steps.

We suggest that another effect, not only diffusion, may help to drive the nanofinger formation process. Guo et al.[13b] performed nanoscale surface modification of the Au(111) surface by scanning the STM tip. Keeping the tunnel voltage unchanged (about 1.5 V), but increasing the tunnel current from less than 0.1 nA to 30 nA, they succeeded in modifying the surface step. At the initial stage the step was changed by extracting atoms by the STM tip. This process required a strong electric field below the STM tip: reduction of the bias to 0.1 V while keeping the tunneling current constant at 30 nA sufficed to prevent atom extraction. After formation of a finger its length was increased with repeated scanning. They suggested that the increase in finger length comes from two contributions: 1) The extraction of atoms from the step edge that connects the base of two neighboring fingers, and 2) the atom attachment to the fingertips. They verified that atom extraction from a step edge requires a high electric field below the STM tip (1.0 V, 30 nA), while atom attachment to the fingertips can occur under normal scanning conditions (1.0 V, 0.1 nA) because gold atoms on the surface diffuse. The initial atom-extraction process also transferred a large number of gold atoms to the tip and subsequently these atoms were redeposited to the substrate thus contributing to the growth of the fingers.

The construction of ZnTBPP functionalized gold fingers in our case did not require the initial step of extraction of gold atoms from the surface at high electric field because adhesion between the Au atoms within the top layer and between the top and second layers was already weakened by the molecules and a very weak electric field was needed to trigger the clusters' mobility.

4. Conclusions

In summary, randomly oriented porphyrins and thiols can assist in the movement of assemblies of gold clusters on the surface under the effect of the electric field induced by the tip. Density functional theory calculations showed that organic

small NANO MICRO

molecules anchoring through sulfur on Au surfaces weaken the interaction between the first two gold layers. At the step edge the assemblies form nanofingers of gold, covered by ZnTBPP molecules, the optical properties of which are known. In principle, this method can be applied to prepare devices where the spectroscopic response of chromophores is increased by 1D gold structures.

5. Experimental Section

Chemicals and solvents: ZnTBPP was synthesized by following the standard procedure[22] for the metal-free porphyrin, using zinc(II) acetate to insert Zn inside the ring. 4-ATP was purchased from Aldrich. Analytical-grade ethanol and chloroform were used as solvents. Chloroform was purified by filtration through a column of basic alumina.

Formation of an SAM of 4-aminothiophenol: The gold (111) substrate, on mica, was purchased from Molecular Imaging, annealed by ethanol flame and cooled under a nitrogen stream. The substrates were immersed into an ethanol solution of 4-ATP (10^{-3} M) for 2 h. The prepared SAM on gold was rinsed with the solvent and dried with nitrogen.

Preparation of porphyrin thin films by axial co-ordination: Ligation with the amino group of 4-ATP SAM on gold was achieved by immersing the 4-ATP SAM on gold into a chloroform solution of ZnTBPP (10^{-4} M) for approximately 72 h. The resulting film was rinsed with chloroform and dried with nitrogen.

STM and STS measurements: The STM measurements were performed using an Omicron VT-STM. The samples were inserted into the vacuum chamber via a fast-entry lock and were therefore not subjected to baking. STM was carried out in ultrahigh vacuum ($\approx 10^{-10}$ mbar) at room temperature using Pt/Ir tips. Tip quality was tested by acquiring atomically resolved images of graphite. STM images were acquired in constant-current mode using tip biases ranging from ± 0.2 to ± 1 V and set points of 0.8 and 0.5 nA. During spectroscopy measurements the feedback loop was switched off and the set-point current, which sets the tip–sample distance, was fixed during the bias scan. The spectroscopy measurements (I–V) were performed by collecting grids of points spaced by 5 nm over scan areas of 200 × 200 nm. The STS spectra shown in this work are averaged over a set of several I–V curves in the grid over the scanning area.

Photoemission and NEXAFS measurements: Photoemission measurements were taken at an emission angle of 30° on the SGM undulator beamline at the Canadian Light Source, Saskatoon, Canada, using a Scienta 100-mm hemispherical analyser. The combined resolution of beamline and analyzer was 160 meV for S 2p and N 1s measurements, measured using the Fermi level of Au, and around 1 eV for the Zn 2p measurements. The photon flux was measured using a calibrated photodiode. Samples were introduced via a load lock. NEXAFS spectra, at room temperature, were taken using the BEAR beamline at the ELETTRA synchrotron, Trieste, Italy.[23] Samples were introduced into the vacuum system via a load lock. The sample-mounting geometry used is reported in Reference [16]. A cylindrical mirror analyzer was used to acquire the NEXAFS spectra, employing Auger yield, with a photon-energy resolution of 0.3 eV.

Computational details: We performed ab initio DFT calculations using the plane-waves code PWSCF.[24] UltraSoft Pseudopotentials[25] were chosen, with wave-function and charge-density cutoff of 40 Ryd and 350 Ryd, respectively. The PW91 parametrization[26] for the exchange-correlation potential was used. We modeled nanoclusters by a small cluster of 4 Au atoms adsorbed on a slab of 4 layers of gold, with a surface unit cell of 12 Au atoms (surface area of 90 Å^2), which ensures a minimum lateral distance between clusters of 5.2 Å. In order to describe the 4-aminothiophenol adsorption on gold we used a short-chain alkanethiol, the methanethiol, adsorbed in the preferential bridge site.[27–28] We extracted the initial gold slab from a fully relaxed 7-layer slab and fixed all the positions, while we allowed the geometric relaxation of both adsorbed cluster and molecule. The systems were placed in a large supercell, with a vertical distance between different units of more then 30 Å, to avoid spurious interactions between slabs.

Acknowledgements

We thank the MIUR FIRB project "Molecular Devices" for funding and the BEAR staff, particularly Bryan Doyle, for assistance at ELETTRA. Part of the research described in this paper was performed at the Canadian Light Source, which is supported by NSERC, NRC, CIHR, and the University of Saskatchewan. Theoretical calculations were performed at the ISUFI-CACT (Lecce). We thank the SPACI consortium for providing computational facilities. The theoretical work was supported by the European project SA-NANO (contract number STRP 013698).

[1] C. A. Hunter, J. K. M. Sanders, *J. Am. Chem. Soc.* **1990**, *112*, 5525.
[2] T. Malinski, Z. Taha, *Nature* **1992**, *358*, 676.
[3] C. H. M. Maree, S. J. Roosendaal, T. J. Savenije, R. E. I. Schropp, T. J. Schaafsma, F. H. P. M. Habraken, *J. Appl. Phys.* **1996**, *80*, 3381.
[4] Y. Harima, H. Okazaki, Y. Kunugi, K. Yamashita, H. Ishii, K. Seki, *Appl. Phys. Lett.* **1996**, *69*, 1059.
[5] P. E. Burrows, S. R. Forrest, S. P. Sibley, M. E. Thompson, *Appl. Phys. Lett.* **1996**, *69*, 2959.
[6] Y. Hamada, *IEEE Trans. Electron Devices* **1997**, *44*, 1208.
[7] M. A. Baldo, D. F. O'Brien, Y. You, A. Shoustikov, S. Sibley, M. E. Thompson, S. R. Forrest, *Nature* **1998**, *395*, 151.
[8] C.-Y. Liu, H.-I. Pan, M. A. Fox, A. J. Bard, *Science* **1993**, *261*, 897.
[9] J. M. Lupton, *Appl. Phys. Lett.* **2002**, *81*, 2478.
[10] J. R. Reimers, T. X. Lu, M. J. Crossley, N. S. Hush, *Nanotechnology* **1996**, *7*, 424.
[11] a) H. S. Yoon, S. J. Park, J. E. Lee, C. N. Whang, I.-W. Lyo, *Phys. Rev. Lett.* **2004**, *92*, 096801; b) I. Matsuda, M. Hengsberger, F. Baumberger, T. Greber, H. W. Yeom, J. Osterwalder, *Phys. Rev. B* **2003**, *68*, 195 319; c) R. Losio, K. N. Altmann, F. J. Himpsel, *Phys. Rev. Lett.* **2002**, *85*, 808; d) M. Shibata, I. Sumita, M. Nakajima, *Phys. Rev. B* **1998**, *57*, 1626.
[12] A. G. Brolo, C. J. Addison, *J. Raman Spectrosc.* **2005**, *36*, 629.

[13] a) F. Yin, R. E. Palmer, Q. Guo, *Surf. Sci.* **2006**, *600*, 1504; b) Q. Guo, F. Yin, R. E. Palmer, *Small* **2005**, *1*, 76.
[14] a) J. M. Keel, J. Yin, Q. Guo, R. E. Palmer, *J. Chem. Phys.* **2002**, *116*, 7151; b) Q. Jin, J. A. Rodriguez, C. Z. Li, Y. Darici, N. J. Tao, *Surf. Sci.* **1999**, *425*, 101.
[15] F. A. Cotton, G. Wilkinson, *Advanced Inorganic Chemistry*, 5th Edition, Wiley, New York 1988.
[16] a) V. Arima, E. Fabiano, R. I. R. Blyth, F. Della Sala, F. Matino, J. Thompson, R. Cingolani, R. Rinaldi, *J. Am. Chem. Soc.* **2004**, *126*, 16 951; b) V. Arima, F. Matino, J. Thompson, R. Cingolani, R. Rinaldi, R. I. R. Blyth, *Surf. Sci.* **2005**, *580*, 63; c) V. Arima, R. I. R. Blyth, F. Della Sala, R. Del Sole, F. Matino, G. Mele, G. Vasapollo, R. Cingolani, R. Rinaldi, *Mat. Sci. Eng. C* **2004**, *24*, 569.
[17] Z.-P. Shi, Z. Zhang, A. K. Swan, J. F. Wendelken, *Phys. Rev. Lett.* **1996**, *76*, 4927.
[18] W. Fan, X. G. Gong, W. M. Lau, *Phys. Rev. B* **1999**, *60*, 10 727.
[19] a) O. S. Trushin, P. Salo, T. Ala-Nissila, *Phys. Rev. B* **2000**, *62*, 1611; b) C. M. Chang, C. M. Wie, S. P. Chen, *Phys. Rev. Lett.* **2000**, *85*, 1044.
[20] a) F. Rosei, M. Schunack, P. Jiang, A. Gourdon, E. Laegsgaard, I. Stensgaard, C. Joachim, F. Besenbacher, *Science* **2002**, *296*, 328; b) J. K. Gimzewski, C. Joachim, R. R. Schlittler, V. Langlais, H. Tang, I. Johannsen, *Science* **1998**, *281*, 531; c) M. Bohringer, W. D. Schneider, R. Berndt, K. Glockler, M. Sokolowski, E. Umbach, *Phys. Rev. B* **1998**, *57*, 4081.
[21] T. Okajima, Y. Yamamoto, Y. Ouchi, K. Seki, *J. Elect. Spectr. Relat. Phenom.* **2001**, *114*, 849.
[22] A. Adler, F. R. Longo, W. Shergalis, *J. Am. Chem. Soc.* **1964**, *86*, 3145.
[23] a) S. Nannarone, F. Borgatti, A. DeLuisa, B. P. Doyle, G. C. Gazzadi, A. Giglia, P. Finetti, N. Mahne, L. Pasquali, M. Pedio, G. Selvaggi, G. Naletto, M. G. Pelizzo, G. Tondello, *AIP Conference Proceedings* **2004**, *705*, 450; b) I. Pasquali, M. Pedio, G. Selvaggi, S. Nannarone, G. Naletto, *ELETTRA News* **2003**, *47* (September).
[24] S. Baroni, A. D. Corso, S. de Gironzoli, P. Giannozzi, http://www.pwscf.org/
[25] D. Vanderbilt, *Phys. Rev. B* **1990**, *41*, 7892.
[26] J. P. Perdew, *Physica B* **1991**, *172*, 1.
[27] Y. Yourdshahyan, A. M. Rappe, *J. Chem. Phys.* **2002**, *117*, 825.
[28] D. Fragouli, T. Kitsopoulos, L. Chiodo, F. Della Sala, R. Cingolani, S. Ray, R. Naaman, *Langmuir* **2007**, *23*, 6156.
[29] L. Scudiero, D. E. Barlow, U. Mazur, K. W. Hipps, *J. Am. Chem. Soc.* **2001**, *123*, 4073.
[30] W. Deng, K. W. Hipps, *J. Phys. Chem. B* **2003**, *107*, 10 736.
[31] G. Polzonetti, A. Ferri, M. V. Russo, G. Iucci, S. Licoccia, R. Paolesse, *J. Vac. Sci. Technol. A* **1999**, *17*, 832.
[32] T. Okajima, Y. Yamamoto, Y. Ouchi, K. Seki, *J. Elect. Spectr. Relat. Phenom.* **2001**, *114*, 849.
[33] M. Konôpka, R. Rousseau, I. Štich, D. Marx, *J. Am. Chem. Soc.* **2004**, *126*, 12 103.
[34] M. C. Vargas, P. Giannozzi, A. Selloni, G. Scoles, *J. Phys. Chem. B* **2001**, *105*, 9509.
[35] H. Kondoh, C. Kodama, H. Sumida, H. Nozoye, *J. Chem. Phys.* **1999**, *111*, 1175.
[36] W. Deng, D. Fujita, T. Ohgi, S. Yokoyama, K. Kamikado, S. Mashiko, *J. Chem. Phys.* **2002**, *117*, 4995.

Received: April 20, 2007
Revised: September 3, 2007
Published online: March 18, 2008

